

Piecewise Convergence Behavior of the Condensed Transfer Function Approach for Mid-to-high Frequency Modelling of a Panel-Cavity System

Zhongyu HU¹, Laurent MAXIT² and Li CHENG^{1*}

¹Department of Mechanical Engineering, The Hong Kong Polytechnic University,
Hung Hom, Kowloon, Hong Kong, China

²Laboratoire Vibrations Acoustique, INSA Lyon, 25 bis, avenue Jean Capelle, 69621
Villeurbanne Cedex, FRANCE

*Corresponding author: li.cheng@polyu.edu.hk

Abstract

The vibro-acoustic modelling of a panel-cavity system is of prime importance for the building industries, exemplified by the noise insulation of single or double skin façade. The vibro-acoustic analysis of such systems in the mid-to-high frequency range is computational costly and technically challenging due to the complex wavelength composition. In the present paper, the Condensed Transfer Function (CTF) approach is revisited to tackle this problem. It is demonstrated that the calculation efficiency of the CTF method can be greatly increased by properly selecting the Condensation Functions (CFs) and exploiting their physical characteristics. In particular, owing to their spatial wavy features, the complex exponential functions can better match the structural wavelength variations so that the velocity on the plate-cavity interface can be described by using a much reduced CF set as compared with the gate functions which are widely used in the previous works. Numerical results show a piecewise convergence behavior of the calculation which is further exploited for establishing a criterion for the truncation of the CFs. The proposed criterion allows the determination of a sub-set of the CFs for any prescribed frequency band for the calculation of the system response in a progressive and piecewise manner, resulting in a great increase in the computational efficiency.

Key words: vibro-acoustic; substructure method; mid-to-high frequency

1. Introduction

The modelling of the noise insulation of building façades usually involves the vibro-acoustic interaction between panels (representing glasses or concrete walls) and cavities (representing rooms or inner cavities between glasses), typically in the frequency range [100 Hz – 5 kHz]. In the current state-of-the-art, most existing evaluations on the acoustic performances of façades and windows are based on simple empirical formulas. When compared with the actual experimental data, however, these formulas are shown to be too approximate to meet the need for allowing parameter variations at the design stage [1]. Meanwhile, accurate modelling tools such as the finite element method (FEM) are extremely computational costly to be used for optimization purposes. Therefore, the lack of proper simulation and optimization tools which are capable of handling rooms of large size with high modal densities in the mid-to-high frequency range is a big challenge.

This problem of general relevance is investigated in this paper by adopting a representative configuration comprising a rectangular cavity coupled with a flexible panel to simulate a typical room. The framework of this study is based on the Condensed Transfer Function (CTF) approach [2] which has already shown its ability and versatility in partitioning complex vibro-acoustic problems like panel-cavity systems. In the CTF approach, the sub-systems are first separately modelled by decomposing the interaction force and the velocities on the interface over a set of basis functions, referred to as condensation functions (CFs). The sub-system models are then assembled based on the force equilibrium and velocity continuity conditions on their interface. To increase the efficiency of the method to reach the mid-to-high frequency, an interface model reduction technique is proposed by reducing the number of CFs used

in the calculation.

The development of dedicated methods for the mid-to-high frequency vibro-acoustic modelling has always been a challenge. Main challenges root in filling the gap left over by the low frequency methods like modal-based methods [3] or the finite element method (FEM)[4-6] and the high-frequency statistical energy analyses (SEA)[7-9]. Assumptions and approximations adopted in these methods are well established, which define and limit their respective application ranges at the same time. In the mid-to-high frequency range, the presence of the short wavelength components challenges the conventional deterministic modelling methods by the exorbitant computational cost incurred. The long wavelength ones, however, fail to meet the SEA assumptions, due to the insufficient modal overlap and the unavailability of the rigorous coupling loss factors[10]. For instance, for the double skin façades, the inner cavity between the two glasses and the internal thick glass may have a low modal density whereas the acoustic room may exhibit thousands of modes within the same frequency range.

In recent years, several strategies have been adopted for tackling the mid-frequency problems. Some attempts consist in reducing the frequency limit of the higher frequency methods like the SEA method, exemplified by Statistical modal Energy distribution Analysis (SmEdA) [11]. The method consists in relaxing the modal energy equipartition assumption used in the traditional SEA. Instead of using the power balance between subsystems used in the SEA, the power balance equations between the resonant modes of different subsystems are established. Circumventing modal energy equipartition allows the handling of subsystems with a relatively low modal overlap[11], as well as the evaluation of the spatial distribution of the energy density within subsystems[12]. Other enhanced SEA methods include energy finite element analysis

(EFEA) [13], which improves the SEA by allowing the damping and the excitation to be spatially distributed over a system. However, similar to other methods based on SEA, the EFEA is limited by the requirement of high modal density, thus hampering its use in the mid-frequency range. Another typical type of approach consists in combining different methods by capitalizing on their respective advantages based on the structural fuzzy theory[14]. Typically, a complex system is divided into a master structure and fuzzy attachments, which can be modelled by different methods. For instance, in the hybrid FEM-SEA approach [15], subsystems with long wavelengths are described by FEM whereas those with short wavelengths by the SEA. These hybrid methods allow adding more details to the classical SEA model whilst avoiding the handling of the entire system by the FEM.

Another typical strategy consists in extending the application range of the low-frequency methods to higher frequencies. The Trefftz methods such as the wave-based method (WBM) [16] and the Variational Theory of Complex Rays (VTCR) [17] are typical examples. In these methods, approximate solutions of the global response are developed using exact solutions of the subsystem motion equations as shape functions and by respecting the boundary conditions between subsystems through a weak formulation. In general, the size of the resultant model is much smaller than that of the equivalent FE model, so as to reach the mid-frequency range. Various versions of such methods exist depending on the choice of the shape functions and the way the boundary conditions and the coupling between subsystems are handled. The Component Modal Synthesis (CMS) models [18] were developed to speed up finite element computations and then to increase the frequency range of applicability of this method. Each component is separately treated in terms of its uncoupled modes and the components are then assembled using basis functions defined on the interface. There is a large

amount of literature devoted to CMS models. Only a few presentative works are cited here. For example, Craig [19] compares the efficiency of using different component modes and concludes that the models based on interface constraint modes together with the fixed-interface normal modes are the most effective. In the early form of the CMS method, the number of constraint modes is equal to the number of degree of freedom at the subsystem interface. For subsystems coupled continuously along a line or a surface (like for acoustic building applications), the number of interface modes can become prohibitive. In order to reduce the degrees of freedom along the coupling interface, a modal-based approach [20] was proposed to describe the mid-frequency vibration transmission from a long-wavelength source and a short-wavelength receiver using the uncoupled free-interface modes. Different examples also include the generalized-interface-dofs method [21] or the characteristic-constraint modes method [18]. Mace and Shorter [22] proposed a local modal/perturbational method that takes the uncertain properties of the considered system into account for the mid-to-high frequency analyses. Uncertainty is introduced at the subsystem level. A perturbation technique relates small changes in the local modal properties to those in the global modal properties. A Monte Carlo simulation is then used to estimate the variability of the frequency response function statistics. This approach was applied to coupled rods.

The Patch Transfer Function (PTF) method [23] was developed for partitioning acoustic [22] or vibro-acoustic [23, 24] problems for enlarging the frequency range of the vibro-acoustic simulation. The method divides the interface into patches using a wavelength-based criterion. For each subsystem, the uncoupled transfer functions between each pair of patches need to be calculated, *a priori*, before being assembled in the final stage. PTF can be seen as an extension of the well-known receptance approach which is commonly used in dynamic analyses for assembling point-coupled mechanical

structures. The PTFs can be calculated by different means. For instance, for subsystems of finite sizes, they can be calculated from the subsystem modes for simple geometry or from the finite element method for complex geometry. For infinitely large acoustic subsystems, they can be estimated from boundary element method or the Rayleigh integral as in [22, 25], or be measured as in [24] for characterizing poroelastic materials used in automotive.

Though intuitive, question still remains on whether discretization by patches is the best way forward in terms of calculation efficiency. In fact, for the modelling of large systems, such as the noise transmission through a building of practical size, the number of patches (i.e. the degree of freedom in the discretized system) may be very large when reaching the mid-to-high frequency range. This makes the direct application of the PTF method difficult, if not impossible. To tackle this issue, attempts were made to extend the PTF approach to further explore other types of discretization schemes, aiming at reducing the number of degree of freedoms and increasing the computation efficiency. As a typical example, the CTF approach generalizes the patches, i.e. the basis functions, of the PTF approach to any function sets over the coupling junction such as the complex exponential functions and the Chebyshev polynomials. The sub-system motions, which will be referred to as condensed velocities, are decomposed in terms of the CFs and assembled together along the interface based on continuity conditions. Up to now, the CTF approach has only been applied to the modelling of the interaction between two line-coupled vibrating mechanical systems, exemplified by the coupling between two panels [2] and a naval application involving a cylindrical shell coupled with non-axisymmetric internal frames [25]. Its application to surface coupled vibro-acoustic system, with the inherently more complex wavelength mixing, has not been dealt with yet.

These problems motivate the present work. We aim at exploring ways to increase the calculation efficiency of the CTF method without losing its accuracy by reducing the interface degrees of freedom, i.e. the number of CFs for the presented method. Firstly, the basic theory of the CTF approach is recalled using a benchmark problem comprising a panel-cavity system. The panel is first assumed to be simply supported so that the system provides analytical solutions for model validation purposes. Clamped case will be considered at a later stage. Through numerical studies, the ability of the CTF method to model the structural-acoustic interaction is verified. Two types of CFs (gate functions and complex exponential functions) are investigated and compared in terms of the modelling efficiency and accuracy. In particular, the advantages of the complex exponential functions are highlighted and explained in terms of their physical wavelength matching characteristics. A selection criterion of the CFs is then proposed, aiming at boosting the CTF method for the mid-to-high frequency simulations. The proposed criterion allows the use of a suitably chosen and reduced CF sub-set to significantly reduce the number of degree of freedom of the system on one hand, and to allow the calculation in a piecewise manner in different frequency bands on the other hand. All in all, this allows an effective and accurate simulation of the panel-cavity system in the mid-to-high frequency range.

2. Formulation

For the completeness, the basic theory of the CTF method is briefly summarized using a benchmark panel-cavity system. Examples of the CTFs are given, and their convergence conditions are introduced. Note that the CTF method is a generalized version of the previous PTF method.

2.1 Basic theory of the CTF method

Consider a rectangular acoustic cavity with one of its walls being covered by a vibrating panel while the others being acoustically rigid, as shown in Fig. 1. The panel is subjected to a prescribed harmonic sound pressure excitation P^e with an angular frequency ω . The two subsystems, structural (panel) and acoustic (cavity), denoted by superscript s and a , respectively, are coupled over their interface Ω which is two dimensional.

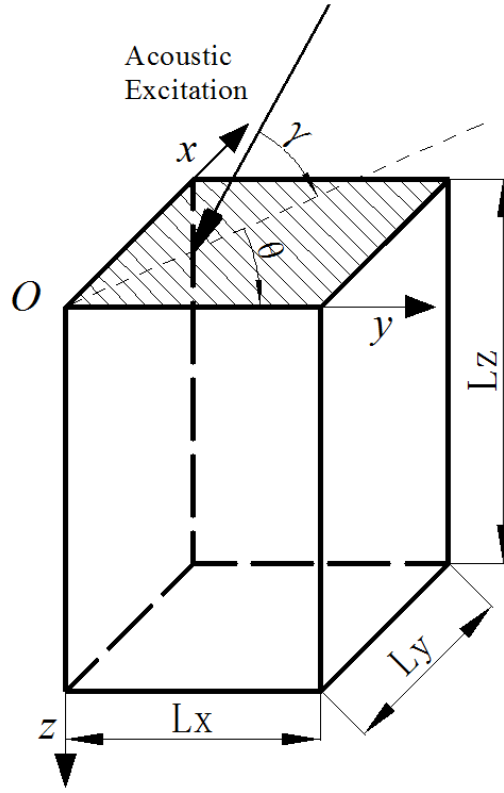


Fig. 1. The panel-cavity configuration and coordinate system

A set of $N_x \times N_y$ orthonormal functions $\{\varphi_{pq}\}_{1 \leq p \leq N_x, 1 \leq q \leq N_y}$, referred to as *Condensation Functions* (CF), is employed to approximate the velocities and the forces on the coupling interface Ω . The value of N_x and N_y should warrant the convergence of the results, which will be discussed later. In the present case, the CFs may be written in a separable form as $\varphi_{pq}(x, y) = \varphi_p(x)\varphi_q(y)$, although the separable form is not a

necessary requirement of the general CTF approach. One assumes that the velocity $U^\alpha(x, y)$ and the force $P^\alpha(x, y)$ can be approximated by the condensation functions for each subsystem α ($\alpha \in [s, a]$) with a sufficient accuracy.

For the structural subsystem, the condensed mobility between φ_{pq} and φ_{kl} defined and calculated as:

$$Y_{kl,pq}^s = \frac{\langle \bar{U}_{pq}^s, \varphi_{kl} \rangle}{\langle P^s, \varphi_{pq} \rangle} = \langle \bar{U}_{pq}^s, \varphi_{kl} \rangle, \quad (1)$$

in which $\langle f, g \rangle$ is a scalar product defined as $\int_{\Omega} f(x, y)g^*(x, y)dS$ with g^* being the complex conjugate of g , and \bar{U}_{pq}^s is the uncoupled normal velocity on Ω when the structural subsystem is subjected to an external excitation $P^s(x, y) = \varphi_{pq}(x, y)$. Additionally, the uncoupled condensed free velocity \tilde{u}_{pq} of the structural subsystem is defined by

$$\tilde{u}_{pq}^s = \langle \tilde{U}^s, \varphi_{pq} \rangle, \quad (2)$$

where \tilde{U}^s is the uncoupled velocity of the structural subsystem over Ω when only an external excitation exists.

For the acoustical subsystem, the condensed impedance $Z_{kl,pq}^a$ is defined as:

$$Z_{kl,pq}^a = \frac{\langle \bar{P}_{pq}^a, \varphi_{kl} \rangle}{\langle U^a, \varphi_{pq} \rangle} = \langle \bar{P}_{pq}^a, \varphi_{kl} \rangle \quad (3)$$

with \bar{P}_{pq}^a being the uncoupled acoustic pressure on Ω when the acoustical subsystem is subjected to the prescribed velocity $U^a(x, y) = \varphi_{pq}(x, y)$. Similarly, the uncoupled condensed free acoustic pressure \tilde{p}_{pq} of the acoustical subsystem is defined by

$$\tilde{p}_{pq}^a = \langle \tilde{P}^a, \varphi_{pq} \rangle, \quad (4)$$

where \tilde{P}^a is the uncoupled acoustic pressure of the acoustical subsystem at Ω when

only the internal sound sources exist. In the present case, this value is null.

Then one can approximate the normal velocity and the normal force distribution on the interface for each subsystem $\alpha \in [s, a]$ as:

$$\left\{ \begin{array}{l} U^s(x, y) \approx \sum_p \sum_q u_{pq}^s \varphi_{pq}(x, y) \\ U^a(x, y) \approx \sum_p \sum_q u_{pq}^a \varphi_{pq}(x, y) \end{array} \right\}, \text{ and } \left\{ \begin{array}{l} P^s(x, y) \approx \sum_p \sum_q p_{pq}^s \varphi_{pq}(x, y) \\ P^a(x, y) \approx \sum_p \sum_q p_{pq}^a \varphi_{pq}(x, y) \end{array} \right\}, \quad (5)$$

where u_{pq}^α and p_{pq}^α are the amplitudes of normal velocity and the normal force distribution with respect to the condensation function φ_{pq} .

On the other hand, the velocity continuity and force equilibrium principle over the coupling interface write

$$\begin{cases} U^s = U^a \\ p^s = -p^a \end{cases} \quad (6)$$

If CFs are orthogonal, one deduces from Eqs. (5-6) the following relationship:

$$\begin{cases} u_{pq}^s = u_{pq}^a \\ p_{pq}^s + p_{pq}^a = 0 \end{cases} \quad (7)$$

Otherwise, similar, but more complex expression can also be developed to link up the components of different amplitudes of normal velocity and the normal force terms.

The superposition principle for passive linear systems can then be used to write the condensed velocities of the panel u_{pq}^s and the condensed pressure of the cavity p_{pq}^a from the condensed mobility and impedance (see Ref. [2] and [25] for details). From the resulting equations and Eq. (7), a linear equation system is obtained which can be cast into a matrix form as:

$$\left[\mathbf{I} + \mathbf{Y}^s \mathbf{Z}^a \right] \mathbf{U}^c = \mathbf{u}. \quad (8)$$

where \mathbf{U}^c is the unknown vector of the condensed normal velocities, \mathbf{u} is the vector of the condensed free velocities characterizing the external excitations, \mathbf{Y}^s is the matrix of the condensed mobility of the panel, \mathbf{Z}^a is the matrix of the condensed

impedance of the cavity, and \mathbf{I} is an identity matrix. It should be reiterated that the orthogonality property of the CFs is not necessary from a theoretical point of view. However, using the property leads to Eq. (7) and then to an equation system which can be written on a very succinct form (i.e. Eq. (8)). Moreover, it is not a restriction to consider this property as it is easy to orthogonalize a set of non-orthogonal functions with the well-known Gram-Schmidt procedure.

In the current cavity-plate configuration, \mathbf{Y}^s and \mathbf{Z}^a can be obtained using the modal expansion method and the analytical expression of the mode shapes of the panel (when simply-supported) and the cavity, respectively. Since these two quantities are both frequency independent, a database can be established beforehand for each subsystem. For more complex cases when the analytical mode shapes are unavailable, numerical tools like FEM can be employed. For the considered case, the condensed mobility of the panel is given by:

$$Y_{pq,kl}^s = \frac{i\omega}{\rho_s h} \sum_m \frac{C_{pq,m} C_{kl,m}^*}{\Lambda_m (\omega_m^2 - \omega^2 + 2i\xi^s \omega_m \omega)}, \quad (9)$$

where ρ_s is the density of the panel, h is the panel thickness, ξ^s is the damping ratio of the panel assumed to be equal for all the panel modes, ω_m is the natural frequency of the m th panel mode, $\Lambda_m = \int \phi_m^2 dV$ and $C_{pq,m} = \int \varphi_{pq} \phi_m dS$ where ϕ_m is the m th panel mode shape, and S is the area of the panel. Similarly, the acoustic impedances of the cavity \mathbf{Z}^a can be written as:

$$Z_{pq,kl}^a = i\omega \rho_0 c_0^2 \sum_n \frac{C_{pq,n} C_{kl,n}^*}{\Lambda_n (\omega_n^2 - \omega^2 + 2i\xi^a \omega_n \omega)} \quad (10)$$

where ρ_0 is the air density, c_0 is the speed of sound in the air, ξ^a is the damping ratio of the cavity assumed to be equal for all the cavity modes, ω_n is the natural frequency of the n th acoustic mode, $\Lambda_n = \int \phi_n^2 dV$ and $C_{pq,n} = \int \varphi_{pq} \phi_n dS$ where ϕ_n is the n th cavity mode shape, and V is the volume of the cavity. The condensed

mobility and the condensed impedance matrix can be estimated using the analytical expression in Eqs. 9 and 10, respectively. Substituting Eqs. 9 and 10 into Eq. 8, the coupled velocity and the interaction force on the interface can be obtained, respectively, as:

$$\mathbf{U}^c = [(\mathbf{Y}^s)^{-1} + \mathbf{Z}^a]^{-1} \mathbf{P}^e \quad (11)$$

where \mathbf{P}^e is the external excitation written under the CF coordinate. The acoustic pressure at any given point M inside the cavity can then be deduced from:

$$P^a(M) = \sum_p \sum_q Z_{M,pq}^a u_{pq}^a \quad (12)$$

where $Z_{M,pq}^a$ is the acoustic impedance of the cavity between the CFs φ_{pq} and the point M , defined by $Z_{M,pq}^a = \bar{P}_{pq}^a(M)$ with $\bar{P}_{pq}^a(M)$ being the pressure at M when the cavity is excited by a prescribed velocity $U^a(x, y) = \varphi_{pq}(x, y)$ on Ω . This quantity can be estimated similarly to the condensed impedances using a modal expansion.

2.2 Two examples on the condensation functions and their convergence rules

2.2.1 Gate functions

The gate functions are defined as:

$$\varphi_{pq}(x, y) = \begin{cases} \frac{1}{\sqrt{L_{gx}L_{gy}}} & \text{if } (p-1)L_{gx} \leq x \leq pL_{gx}, (q-1)L_{gy} \leq y \leq qL_{gy}, \\ 0 & \text{elsewhere} \end{cases} \quad (13)$$

where L_{gx} and L_{gy} are the lengths of the gate function and p and q are the gate indices in x and y directions, respectively. As illustrated in Fig. 2, each condensed mobility term $Y_{kl,pq}$ physically corresponds to the velocity response U_{kl} when a unit excitation P_{pq} is applied. When the gate functions are employed, the CTF method

retreats to the PTF method as a special case. Owing to the intuitive and explicit physical meaning of the gate functions, the corresponding condensed mobility and impedance can be obtained using various calculation schemes, or even from experimental measurements.

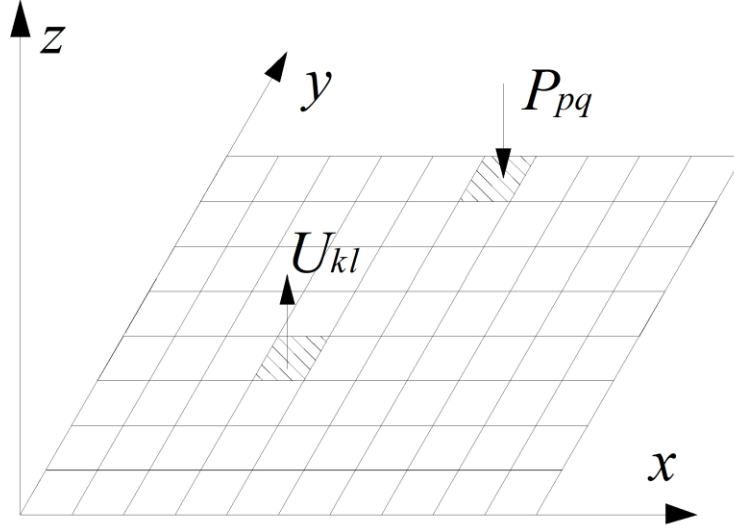


Figure 2. The working principle of gate functions

The convergence criterion for the PTF is well established [23], stipulating that at least two gate functions are needed to describe a wavelength, analogous to the spatial Shannon criterion used in signal processing. Therefore, for a given structural or acoustical wavelength λ , the length of the gate functions L_{gx} and L_{gy} should satisfy:

$$L_{gx} \leq \frac{\lambda}{2}, L_{gy} \leq \frac{\lambda}{2}. \quad (14)$$

2.2.2 Complex exponential functions

The complex exponential functions are given by

$$\varphi_{pq}(x) = \frac{1}{\sqrt{L_x L_y}} \exp(i \frac{2p\pi x}{L_x}) \exp(i \frac{2q\pi y}{L_y}). \quad (15)$$

in which $p \in [0, \pm 1, \pm 2, \dots, \pm I_{max}^x]$ and $q \in [0, \pm 1, \pm 2, \dots, \pm I_{max}^y]$ are the function indices in x and y directions, respectively. Different from the case of the gate functions in which the coupling interface is divided into more intuitive ‘patches’, the

use of the exponential functions spatially decomposes the velocity and the force over the entire coupling interface.

In the following, we will consider a similar convergence criterion than the one proposed in Ref. [25] for the line coupled mechanical structures. In the present case of a panel-cavity system coupled over a surface, it can be expressed as:

$$I_{max}^x \geq \frac{2L_x}{\lambda} - 1 \quad \text{and} \quad I_{max}^y \geq \frac{2L_y}{\lambda} - 1. \quad (16)$$

This criterion will be verified through numerical simulations and analyses hereafter.

3. Analyses and Improvement

In the following numerical analyses, the dimension of the cavity is set to be 2.5m×2m×3m ($x \times y \times z$). The plate is assumed to be simply-supported to facilitate the model validation. The panel is 1.8mm thick, located at $z=0$ forming one wall of the enclosure. The panel is made of glass and it has a Young's modulus 7.2×10^{10} Pa with a Poisson's ratio 0.2 and mass density 2.53×10^3 kg/m³. Damping ratios ξ^a and ξ^s are set to 0.001 and 0.01 for the cavity and the panel, respectively. An oblique acoustic excitation with an amplitude of 20Pa impinges on the panel, with both the dihedral angle and the intersection angle with x axis being 45° (i.e. $\gamma=\theta=45^\circ$ in Fig. 1). The use of the oblique incident excitation ensures the excitation of more panel modes to get the complexity needed for the analyses. The frequency band of interest is [1, 1000] Hz. Additionally, according to Eqs. (14) and (16), the number of the condensation functions should be determined by the shorter wavelength among the subsystems. Because the number used for the two subsystems needs be equal to be assembled together in Eq. (8), the number of functions to be used is then selected according to the subsystem whose wavelength at 1000Hz is shorter. In the present case, the shorter wavelength comes

from the acoustic system with a smallest wavelength of 0.17m. This results in a minimum of 174 condensation functions. In the present case, 180 gate functions will be used (15 for x direction and 12 for y direction) in the calculation. For the complex exponential functions, the convergence criteria Eq. (16) impose $I_{max}^x = I_{max}^y = 6$, giving a total of 169 terms in the calculation.

Table 1 tabulates the number of modes and modal overlap factor in the one-third octave frequency bands. To better quantify the frequency range, we define the start of the so-called mid-frequency range when the modal overlap factor of either subsystem is close to one. In the present case, the so-called mid-frequency domain begins at the third octave band with a center frequency of 500 Hz.

Table 1 Number of modes and modal overlap factor of the panel and the cavity in different one-third octave frequency bands

Center frequency of the 1/3 octave band (Hz)	Number of modes		Modal overlap factor	
	Panel	Cavity	Panel	Cavity
250	3	26	0.21	0.07
315	5	49	0.26	0.21
400	8	94	0.33	0.43
500	10	167	0.41	0.84
630	11	334	0.52	1.69
800	17	634	0.74	3.38
1000	19	1247	0.83	6.77

3.1 Acoustic Pressure

The sound pressure is calculated at an arbitrarily chosen point within the enclosure (0.5, 1.3, 2)m. The calculated sound pressure level (SPL) is given in Fig. 3, in which the results using two different CFs are compared with the reference solution obtained from the analytical results based on the exact wave method, which has been fully validated in a previous paper [26]. It can be seen that the pressure prediction by both

types of CFs agree well with the reference result in the low frequency range. However, the performance of the gate functions slightly deteriorates as compared with their complex exponential counterparts in the higher frequency range, especially at the troughs of the curves where system becomes less dynamic. Similar results are observed when averaging the acoustic pressure within the entire cavity. Generally speaking, the convergence criteria Eqs. (17, 19) ensure acceptable calculation accuracy for both types of CFs.

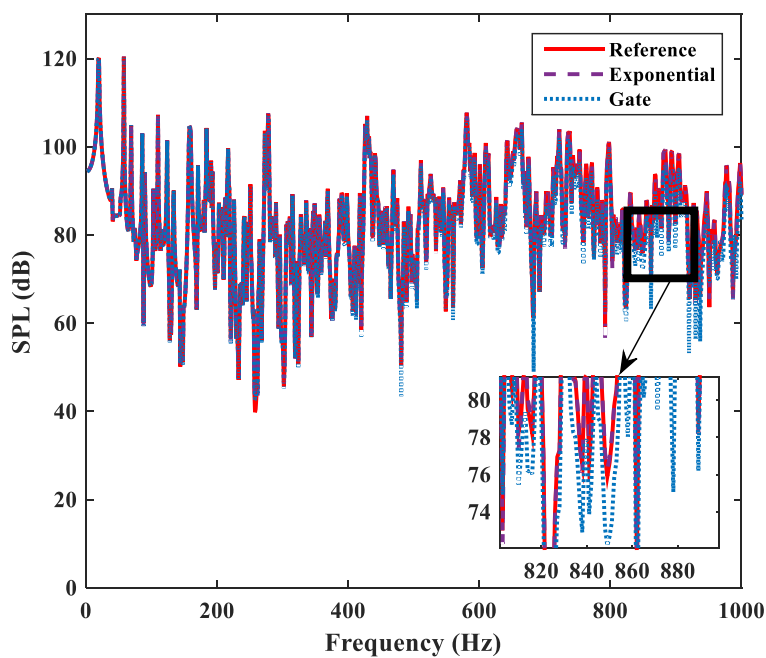


Fig. 3 SPL (with reference to 2×10^{-5} Pa) using two types of CFs compared with reference solutions

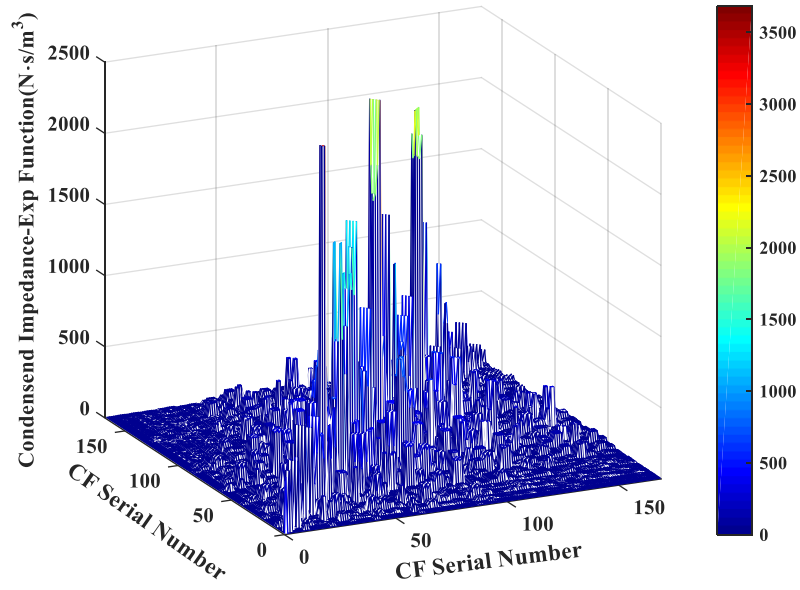
3.2 Analyses of the CTF method

As the CTF method converges similarly whatever the considered CFs are (i.e. gate or complex exponential), some intermediary quantities of the method with different CFs will be investigated in order to reveal properties which could be used to reduce the number of degree of freedom (i.e. number of CFs) and then enlarge the applicable range of CTF to the

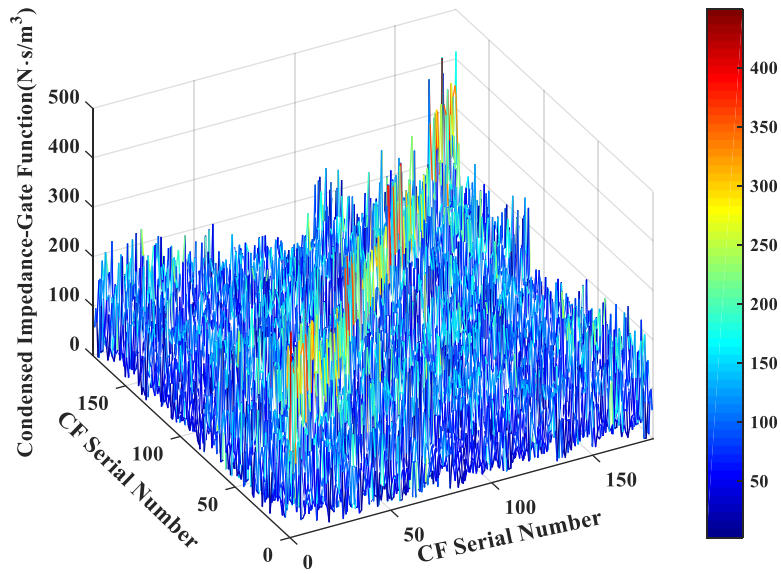
mid frequency range. Two variables are to be analyzed, namely the condensed impedance of the cavity and the condensed normal velocity when the panel is coupled to the cavity. Since these two variables are frequency dependent, a single frequency, 800 Hz, is selected for analyses.

3.2.1 Condensed impedance

For the cavity, the condensed impedance $Z_{kl,pq}^a$ calculated from the complex exponential functions and the gate functions are shown in Figs. 4(a) and 4(b), respectively. The x -axis and y -axis are the serial number of the condensation functions φ_{pq} following the order: $[\varphi_{11}, \varphi_{12}, \dots, \varphi_{1q}, \varphi_{21}, \varphi_{22}, \dots, \varphi_{pq}]$, in which $p, q = [0, 1, 2, \dots]$ for the gate functions and $p, q = [0, 1, -1, 2, -2, \dots]$ for the exponential functions. It is observed in Fig. 4(a) that, for the complex exponential functions, the condensed impedance terms along the diagonal region have much larger values than those on the off-diagonal area. Even this strong coupling within the diagonal region seems to be dominated by a limited number of combinations rather than all diagonal terms. Almost all off-diagonal combinations appear to be so small that they can be neglected during the calculations, revealing the possibility for further approximations with the CTF method. As for the gate functions, Fig. 4(b) shows that the condensed impedance terms are not as concentrated as in the case of the complex exponential functions. All combinations of pq and kl are of comparable importance to be considered during the calculation, leaving less rooms in making further simplifications to increase the calculation efficiency using gate functions. Analyses show similar behaviors for the condensed impedance at other frequencies as well as the condensed mobility (not shown here).



(a)



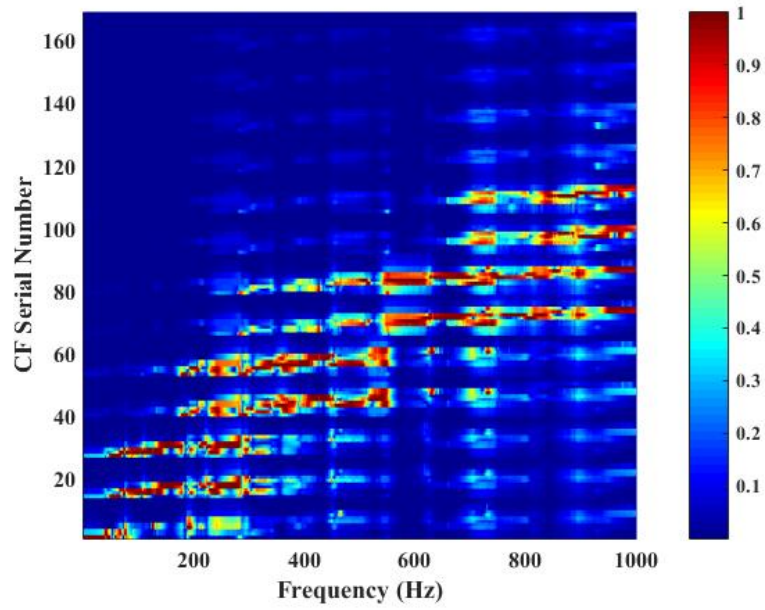
(b)

Fig. 4 Modulus of the condensed impedance between condensation functions: (a) complex exponential functions at 800 Hz; (b) gate functions at 800 Hz.

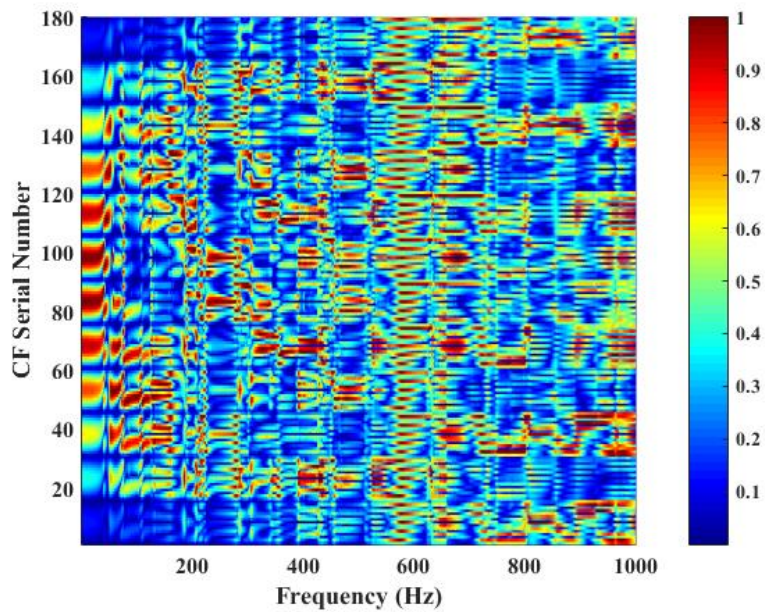
3.2.2 Condensed velocity

The coupling velocity $U(x, y) = \sum_{p,q} u_{pq} \varphi_{pq}(x, y)$ on the interface is analyzed.

u_{pq} represents the contribution from the particular CF term φ_{pq} to the coupled velocity. Figure 5 shows this quantity normalized with respect to the largest value at each frequency, be it for the complex exponential functions or the gate functions, within $[0, 1000]$ Hz. The x -axis is the frequency and the y -axis is again the CTF serial number pq arranged in the same way as in Fig. 4. It can be seen from Fig. 5(a) that, for the complex exponential functions and for each frequency, there always exist some dominant terms holding a higher weight than the others, which are consistent with the behavior of the condensed impedance and the condensed mobility. It can then be surmised that the coupling velocity, which is the key parameter connecting the coupled subsystems, might be estimated by using a small number of CF terms if one knows how to choose them. Additionally, these dominant terms change as the frequency varies. As to the gate functions in Fig. 5(b), at any given frequency, the contributions from different terms are rather uniform, showing no particular dominant pattern. This can be explained by the mathematical properties of the gate functions. Indeed, as opposed to the continuous and wavy feature of the complex exponential functions, gate functions show discontinuities in their spatial distribution. As a result, it is naturally more difficult to map the waveform of the velocity over the interface, unless an increasing number of terms are used. For the complex exponential functions, however, the calculation efficiency could be greatly increased if only dominating terms can be extracted within a frequency band. This will be further exploited hereafter.



(a)



(b)

Fig. 5 Normalized velocity contributions of different condensed functions in the frequency band $[0, 1000]$ Hz: (a) complex exponential functions; (b) gate functions.

3.3 Model reductions using complex exponential functions.

To extract the dominating terms in the complex exponential functions, two

generalized wavelength terms are defined to characterize their wavy nature based on their function wavelength and the wavelength of the vibrating panel or that of the acoustic cavity. It is found that the dominating CF terms have a close tie with the wavelength of the two subsystems. A selection rule for the exponential functions is then proposed accordingly, which allows truncating the series terms by keeping the most dominant ones so that the size of the system matrix $[\mathbf{Y}]$ and $[\mathbf{Z}]$ can be reduced.

3.3.1 Generalized wavelength of the CTF

Two generalized wavelengths λ_{ca} and λ_{cs} are defined to connect the condensation functions with the acoustic cavity and vibrating structural, respectively, as:

$$\lambda_{ca} = \frac{\lambda_{c,pq}}{\lambda_a} \quad (17)$$

$$\lambda_{cs} = \frac{\lambda_{c,pq}}{\lambda_s} \quad (18)$$

where $\lambda_{c,pq}$ is the wavelength of the complex exponential function $\varphi_{pq}(x, y)$, defined as

$$\lambda_{c,pq} = \frac{2\pi}{\sqrt{\left(\frac{2p\pi}{L_x}\right)^2 + \left(\frac{2q\pi}{L_y}\right)^2}}, \quad (19)$$

and λ_a and λ_s are the acoustic wavelength and structural wavelength, respectively, which are frequency dependent. For convenience, those acoustic modes with λ_{ca} smaller than one are referred to as the inertia dominated modes, otherwise, they are called stiffness dominated modes [27]. The same rule also applies to structural modes characterized by λ_{cs} . Using the definition, λ_{ca} and λ_{cs} at 250Hz, 650Hz, and 800Hz are calculated for the complex exponential functions used in the last section and shown in Figs. 6(a), 6(b), and 6(c), respectively. Note that 650Hz is the critical frequency of the panel. In these figures, the y-axis is the $|u_{pq}|$ from each condensation function

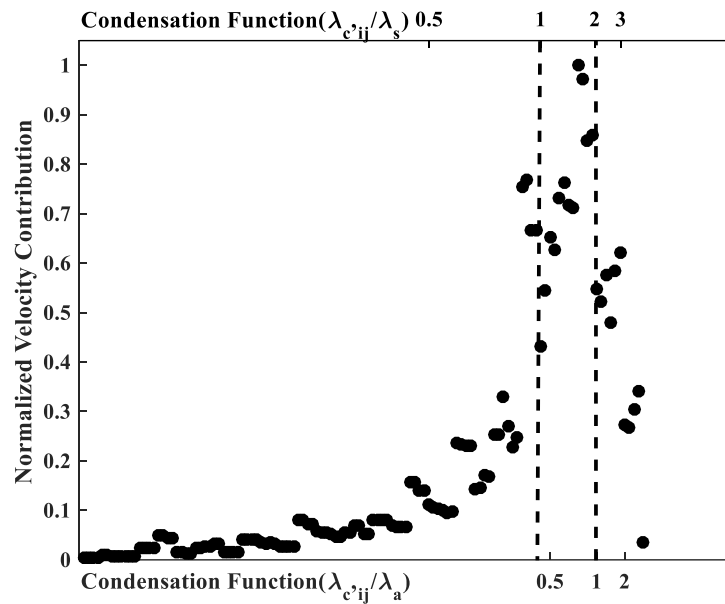
normalized with respect to the largest value of $|u_{pq}|$. Figs. 6(a) and 6(c) have two x -axes, with λ_{cs} on the bottom and λ_{ca} on the top, both being arranged in an increasing order. The sequence of the condensation functions remains the same for the two x -axes, because $\lambda_{c,pq}$ is frequency independent and both λ_a and λ_s are fixed numbers for any given frequency. Fig. 6(b) has only one x -axis since $\lambda_{ca} = \lambda_{cs}$ at the critical frequency.

In Fig. 6(a), two reference dash lines are plotted at $\lambda_{ca}=1$ and $\lambda_{cs}=1$ for the ease of analyses. It can be seen that most of the dominating terms are located around the two reference lines and more on their right side than the left side, which means a more predominant contribution from the inertia modes than the stiffness modes. Comparing the three sub-figures in Fig. 6, it can be seen that this phenomenon occurs at all the three frequencies being analyzed. In Fig. 6(c), more inertia terms are involved when the frequency increases, while the stiffness terms still have little contribution. Particularly in Fig. 6(b), the coupling is strongly dominated by the four terms close to $\lambda_{ca} = \lambda_{cs} = 1$, *i.e.* $\varphi_{\pm 3, \pm 3}(x, y)$ with a function wavelength of 0.521m, as compared with the critical wavelength of the system of 0.523m. This shows that the two subsystems strongly interact at the critical frequency and this strong coupling can be characterized by a very small number of condensation functions with close wavelengths.

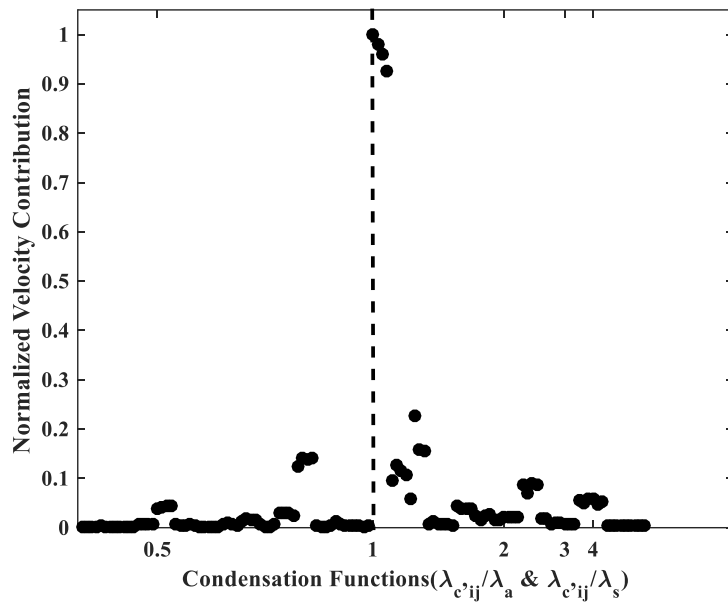
Another noteworthy phenomenon is the location of the term which has the largest contribution. It is closer to $\lambda_{ca}=1$ at the lower frequency (Fig. 6(a)) but much closer to $\lambda_{cs}=1$ at the higher frequency (Fig. 6(c)). This is because 250Hz (Fig. 6(a)) is before the critical frequency in which the acoustic wavelength is larger than that of the panel. Therefore, the acoustic cavity is a large wavelength subsystem, contrary to the supersonic case of 800Hz (Fig. 6(c)).

Generally speaking, it can be concluded that, at any prescribed frequency and

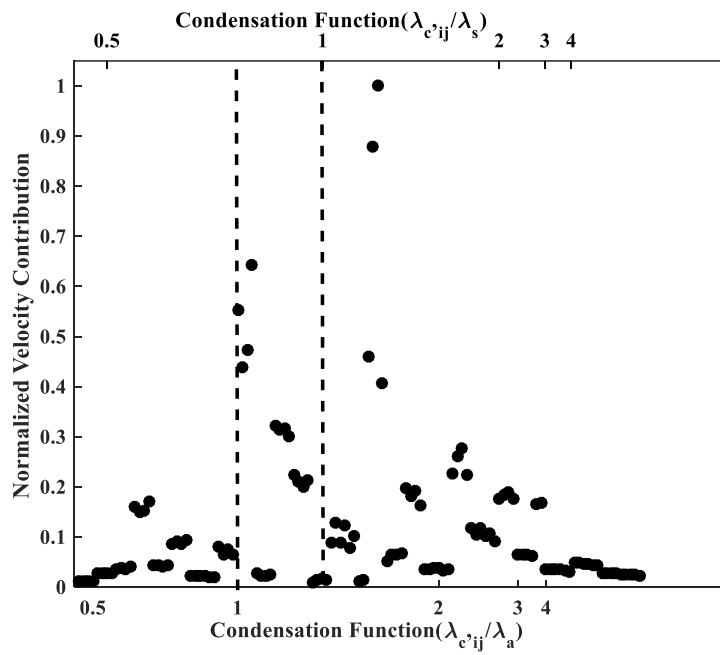
within a band, those CF terms which feature a better spatial wavelength match with the system would dominant the system responses. This explains why complex exponential functions outperform the gate functions in terms of both accuracy and efficiency. It can be surmised that there could be other function sets which are more efficient to model a system if the function wave of which match the structure wave characteristics. For example in an acoustic-black-hole structure, one may use wavelet to achieve a better modelling efficiency [28]. However, it is beyond the scope of this paper and will be explored in the future works.



(a)



(b)



(c)

Fig. 6 Normalized velocity contribution from each complex exponential function, arranged according to their function wavelength with respect to acoustic wavelength and structural wavelength: (a) 250Hz; (b) 650Hz (critical frequency) (c) 800Hz.

3.3.2 A piecewise calculation scheme with CTF method

Before moving forward to the detailed selection criterion, an error quantification can be introduced to evaluate the ability of the CFs to map the velocity field on the coupling surface. An error index is defined for the frequency band $[\omega_1, \omega_2]$ as $20 \log_{10} E_{pq}$ where

$$E_{pq} = \frac{1}{S(\omega_2 - \omega_1)} \int_{\omega_1}^{\omega_2} \int_0^{L_y} \int_0^{L_x} [u_c(x, y, \omega) - \sum_{p,q} u_{pq}(\omega) \phi_{pq}(x, y)]^2 dx dy d\omega \quad (20)$$

in which u_c is the panel velocity obtained from the reference method, i.e. wave approach [26]. Generally, larger p and q could lead to a smaller error but a reduced calculation efficiency.

For a frequency band $[f_l, f_h]$, the corresponding wavelength range of the coupled system is denoted by $[\lambda_h, \lambda_l]$. Three representative scenarios, corresponding to before critical, critical and after critical bands, are listed in Table 2 and analyzed.

Table 2 System critical frequency and the wavelength selection

Frequency band property	Frequency band	Wavelength selection
below critical	$f_l < f_c$ Hz, $f_h < f_c$ Hz	$\lambda_l = \lambda_a$, $\lambda_h = \lambda_s$
critical	$f_l < f_c$ Hz, $f_h > f_c$ Hz	$\lambda_l = \lambda_a$, $\lambda_h = \lambda_a$
above critical	$f_l > f_c$ Hz, $f_h > f_c$ Hz	$\lambda_l = \lambda_s$, $\lambda_h = \lambda_a$

Firstly, the selection criterion should include all dominating terms close to $\lambda_{ca} = 1$ and $\lambda_{cs} = 1$ for all frequencies within the band. That is to say, the wavelengths of the selected exponential functions should cover all the existing wavelengths of the coupled system within the frequency band. Furthermore, as indicated in section 3.3.1, the inertia modes impose a larger weight on the response than the short wavelength terms do. Therefore, more long-wavelength terms should be preserved in the calculation.

Assuming all the condensation functions that should be kept in the calculation have a function wavelength $\lambda_{c,pq}$ to satisfy $\alpha\lambda_h < \lambda_{c,pq} < \beta\lambda_l$, then the coefficient

α and β is delimited by $0 \leq \alpha \leq 1$ and $\beta \geq 1$, respectively. Apparently, a smaller α or a larger β increases the size of the series sub-set, thus providing a better calculation accuracy but a reduced efficiency. In particular, when $\alpha=1$ and $\beta \rightarrow \infty$, the criterion coincides with the traditional convergence rule. Therefore, the dominating terms should be extracted by properly selecting β . Figure 7 shows the calculation errors, which are obtained based on Eq. 21, for three different one-third octave frequency bands with the center frequencies of 630 Hz, 800 Hz and 1000 Hz, respectively. It can be found that the error drops as the value of β increases and the drop speed slows down from $\beta = 1.5$ onwards. Particularly, the error for the 630 Hz band is small even for low value of β . The reason is that the 630 Hz band contains the critical frequency and its wavelength variation is relatively not significant so that the response expression is dominated by on a few terms, which is consistence with the result shown in Fig. 6b. Generally speaking, $\beta = 1.5$ seems to be a good compromise between the accuracy and the calculation efficiency.

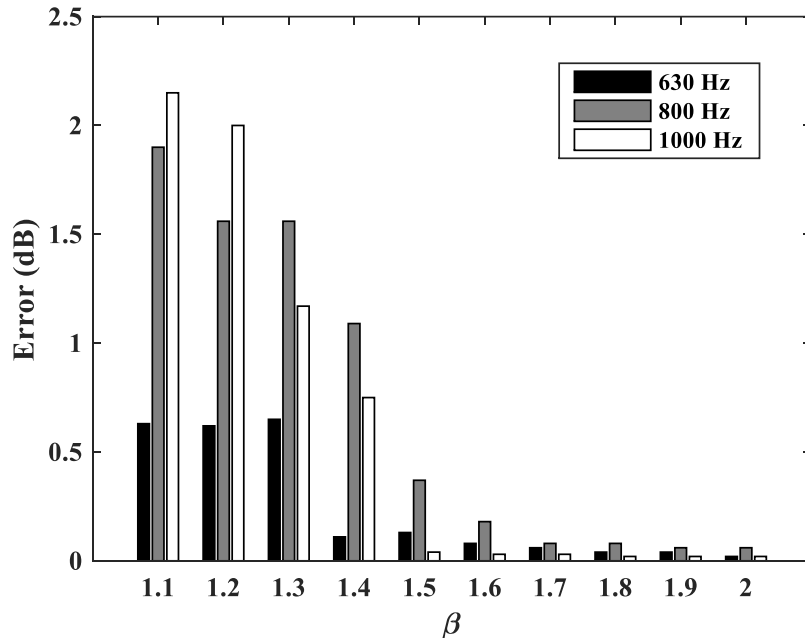


Fig. 7 CTF calculation error for different β values within one-third octave frequency bands: 630 Hz, 800 Hz, and 1000 Hz.

The proposed selection criterion is applied to calculate the overall pressure response of the cavity within the one third octave band with a center frequency of 630Hz, with the results shown in Fig. 8 using $\beta=1.5$. It can be observed that the system responses at the resonance frequencies are well predicted by using only 60 CF terms while the old convergence rule would require 80 terms. Slight discrepancies exist at some non-resonant frequencies especially in the higher frequency part of the band. The corresponding one-third octave band SPL error is calculated, giving 0.13dB within the frequency band contained in Fig. 8. The errors in Eq. 20 and the CF terms used by the proposed criterion and the traditional criterion for other one-third octave bands are listed in Table 3. It can be seen that $\beta=1.5$ leads to a slightly larger but still acceptable accuracy as compared to the case of $\beta=2$ for the all bands in the mid-frequency range (starting from the band of 500 Hz according to the previous definition) with a further-reduced system size. It is expected that the accuracy in the low frequency range may deteriorate because of the insufficient modal density, exemplified by the band below 315Hz. As to the model size, the proposed selection criterion obviously reduces the number of the CF terms used, i.e. the matrix size in Eq. 8, leading to an expected increase in the calculation efficiency. It is understandable that the proposed criterion intends to guaranty the calculation accuracy only within the targeted frequency band, instead of trying to cover the entire frequency range, as shown in Fig. 9(a), in which the lower frequencies are deliberately abandoned. Nevertheless, as shown in Fig. 9(b), the proposed criterion can be applied to any arbitrarily selected bands, one at a time so that the entire frequency range can be covered by moving the bands in a sequential way. This sequential calculation scheme is what the piecewise calculation means. This way, the calculation efficiency can be maximized in each frequency band of interest.

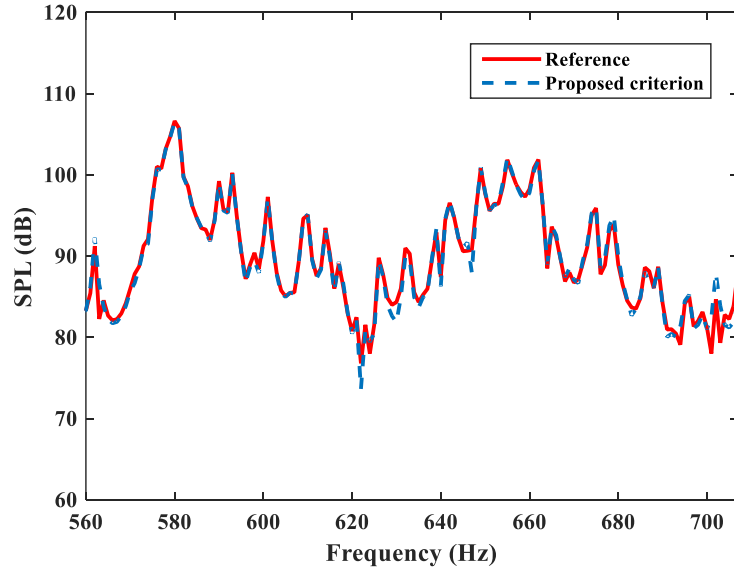
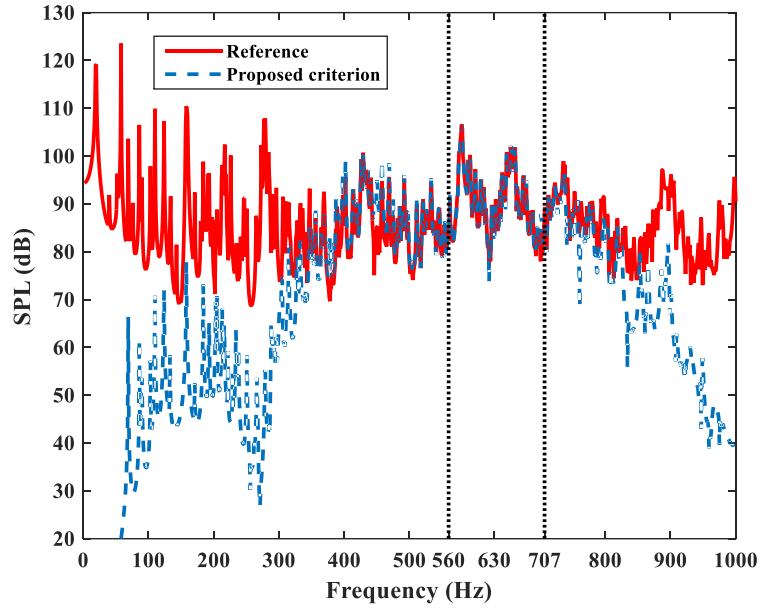


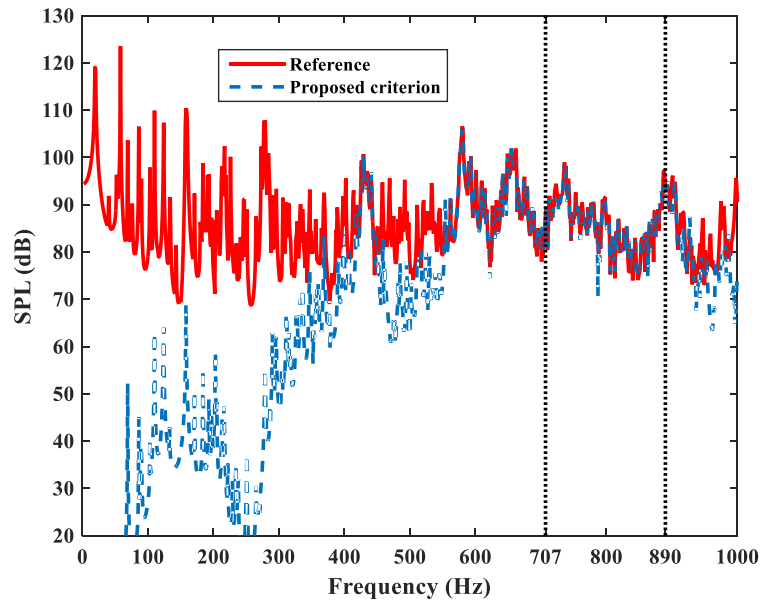
Fig. 8 Calculated SPL using the proposed selection criterion for the one third octave frequency band (center frequency: 630Hz).

Table 3 Performance of the proposed selection criterion

Center frequency of the one third octave bands	Error		Piecewise terms		CTF terms (previous rule)
	$\beta = 1.5$	$\beta = 2$	$\beta = 1.5$	$\beta = 2$	
250 Hz	1.16 dB	0.21 dB	20	22	31
315 Hz	1.14 dB	0.47 dB	26	28	40
400 Hz	0.75 dB	0.52 dB	34	36	51
500 Hz	0.58 dB	0.49 dB	40	42	64
630 Hz	0.13 dB	0.02 dB	50	60	80
800 Hz	0.37 dB	0.06 dB	80	96	137
1000 Hz	0.04 dB	0.02 dB	122	146	218



(a)



(b)

Fig. 9 Sound pressure level using the proposed criterion targeting two selected one-third octave bands with the center frequency: (a) 630 Hz; (b) 800 Hz.

To further assess the performance and the robustness of the proposed criterion, an additional case of a cavity with boundary impedance, coupled to clamped panel, is considered. The impedance wall is located at $y=0$ within the XOZ plane as shown in

Fig. 1, with a normalized acoustic impedance of 33.5 with respect to the characteristic impedance of air $\rho_0 c_0$ [29]. Notice that the sound velocity $c_0 = 340*(1+0.001i)$ is complex. Therefore, the impedance used here is a complex quantity, including both resistance and reactance parts. The changes in the boundary conditions of the cavity serve the purpose of breaking down the symmetrical modal shape of the cavity as well as its spatial matching with the plate over the coupling surface. In this case, the condensed mobility of the panel (Eq. 10) is not obtained analytically. Instead, numerical calculations using FEM are conducted. The impedance boundary can either be treated as a subsystem to be substituted into Eq. 11, or modelled as part of the entire cavity [29]. The former option is adopted in the present case. The calculated frequency band is increased to [1000, 1600] Hz. The volume averaged SPL calculated with $\beta = 1.5$ is compared with the FEM result in Fig. 10. It can be seen that the proposed piecewise calculation scheme predicts well the system response in the entire frequency band of interest. However, one observes discrepancies in regions where the system dynamics are weak. Three factors might result in these errors: higher frequencies, clamped plate boundary and the impedance wall. In Table 3, it can be observed that higher frequencies have little effect on the calculation error. Therefore, the change in the system boundary could be the main contributing factor. The inherent calculation error of the finite element simulation may also be part of the reasons behind these discrepancies. In the present case, the calculation time is also observed to be reduced. To give an indicative idea, the calculation time is rough 1/5 and 1/2 that of the FEM and conventional CTF, respectively. It should be noted that the exact calculation time may vary depending on the computer capability and the case under investigation.

As a final remark, the calculation accuracy using the proposed piece-wise criterion and the time required for dealing with a larger cavity, (5 x 3 x 3) m for instance, is also

tested. Under the same calculation condition as Fig. 8, the same calculation accuracy is achieved, with however a much longer computation time (roughly 20 times). This is obviously due to the significant increase of the modal density in the frequency band.

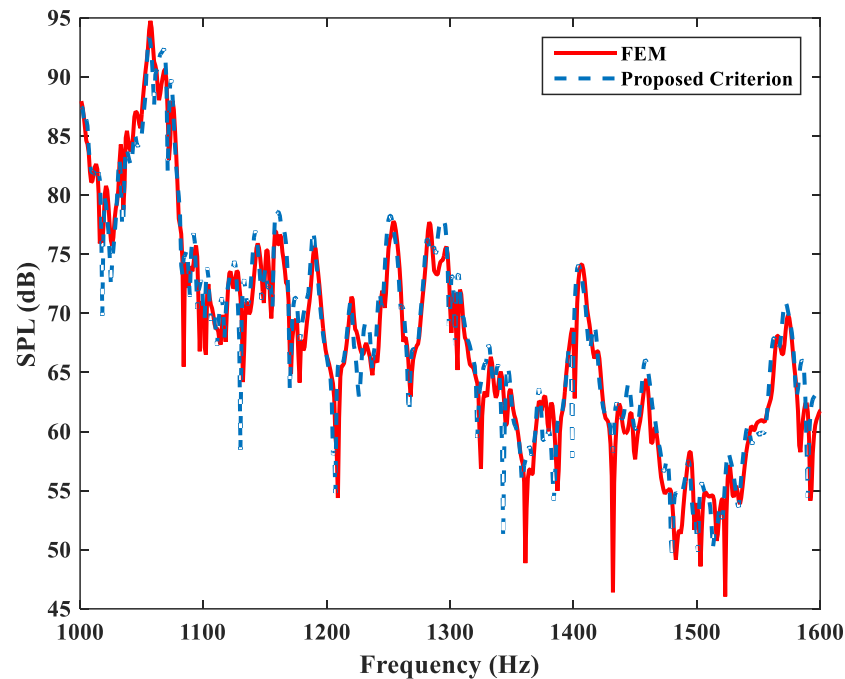


Fig. 10 Sound pressure level using the proposed criterion targeting [1000, 1600] Hz (clamped panel and cavity with impedance boundary).

4. Conclusions

Aiming at achieving an effective modelling of a coupled panel-cavity system in the mid-to-high frequency range, a revisited condensed transfer function method along with a series truncation criterion is proposed in this work. As an example, the originally established line-coupled CTF method is revisited and applied to the modelling of a surface-coupled benchmark vibro-acoustic system comprising a panel and a cavity. The validity of the method is verified through comparisons with the reference solutions, when both the gate functions and the complex exponential functions are used.

Calculation results are found to be similar, albeit small differences, between the two types of the CFs. Meanwhile, a piecewise convergence behavior of the complex exponential function based CTF method is revealed, allowing a model reduction for mid-frequency simulations. This unique feature of the complex exponential functions is attributed to their wavy feature and spatial matching with the dynamics of the physical system. Based on that, a series selection criterion for the complex exponential CFs is proposed to further increase the calculation efficiency. Given a targeted frequency band $[f_l, f_h]$, all complex exponential CFs φ_{pq} with their wavelengths $\lambda_{c,pq}$ delimited by $\alpha\lambda_h < \lambda_{c,pq} < \beta\lambda_l$ are kept to form a subset, to be used in the calculation. It has been shown that using $\alpha=1$ and $\beta=1.5$ can guarantee an acceptable prediction accuracy in most of the analyzed cases. Calculation errors might be larger in some frequency bands but still within the tolerance level typically required for mid-to-high frequency modelling. The most significant advantage of the proposed criterion is that it allows accurate modelling of the system in a piecewise manner in terms of frequency bands at a much-reduced model and calculation cost.

Acknowledgements

The authors thank the Research Grant Council of the Hong Kong SAR for the financial support to the project (PolyU 152017/17E).

Reference

- [1] V. Huckemann, É.B. Leão, and M. Leao, "Acoustic comfort in office buildings with double skin glass façades," *Bauphysik* **31**(5), 305-312 (2009).
- [2] V. Meyer, L. Maxit, J.L. Guyader, T. Leissing, and C. Audoly, "A condensed transfer

- function method as a tool for solving vibroacoustic problems," *Proceedings of the Institution of Mechanical Engineers, Part C: Journal of Mechanical Engineering Science* **230**(6), 928-938 (2015).
- [3] E.H. Dowell, G.F. Gorman, and D.A. Smith, "Acoustoelasticity: General theory, acoustic natural modes and forced response to sinusoidal excitation, including comparisons with experiment," *Journal of Sound and Vibration* **52**(4), 519-542 (1977).
- [4] F.J. Fahy and P. Gardonio, *Sound and structural vibration: radiation, transmission and response*. 2007: Academic press.
- [5] M. Petyt, *Introduction to finite element vibration analysis*. 2010: Cambridge university press.
- [6] B. Pluymers, W. Desmet, D. Vandepitte, and P. Sas, "Application of an efficient wave-based prediction technique for the analysis of vibro-acoustic radiation problems," *Journal of Computational and Applied Mathematics* **168**(1-2), 353-364 (2004).
- [7] R.H. Lyon, *Theory and application of statistical energy analysis*. 2014: Elsevier.
- [8] F.J. Fahy, "Statistical energy analysis: a critical overview," *Philosophical Transactions of the Royal Society of London A: Mathematical, Physical and Engineering Sciences* **346**(1681), 431-447 (1994).
- [9] A. Le Bot, *Foundation of statistical energy analysis in vibroacoustics*. 2015: OUP Oxford.

- [10] A. Le Bot and V. Cotoni, "Validity diagrams of statistical energy analysis," *Journal of Sound and Vibration* **329**(2), 221-235 (2010).
- [11] L. Maxit and J.L. Guyader, "Extension of SEA model to subsystems with non-uniform modal energy distribution," *Journal of Sound and Vibration* **265**(2), 337-358 (2003).
- [12] N. Totaro and J.L. Guyader, "Extension of the statistical modal energy distribution analysis for estimating energy density in coupled subsystems," *Journal of Sound and Vibration* **331**(13), 3114-3129 (2012).
- [13] F. Han, R. Bernhard, and L. Mongeau, "Prediction of flow-induced structural vibration and sound radiation using energy flow analysis," *Journal of Sound and Vibration* **227**(4), 685-709 (1999).
- [14] C. Soize, "A model and numerical method in the medium frequency range for vibroacoustic predictions using the theory of structural fuzzy," *The Journal of the Acoustical Society of America* **94**(2), 849-865 (1993).
- [15] P.J. Shorter and R.S. Langley, "Vibro-acoustic analysis of complex systems," *Journal of Sound and Vibration* **288**(3), 669-699 (2005).
- [16] W. Desmet, P. Sas, and D. Vandepitte, "An indirect Trefftz method for the steady-state dynamic analysis of coupled vibro-acoustic systems," *Computer Assisted Mechanics and Engineering Sciences* **8**(2-3), 271-288 (2001).
- [17] P. Ladevèze, L. Arnaud, P. Rouch, and C. Blanzé, "The variational theory of complex rays for the calculation of medium - frequency vibrations," *Engineering*

- Computations **18**(1/2), 193-214 (2001).
- [18] C. Pierre and M.P. Castanier, *Mid-frequency dynamics of complex structural systems: Assessing the state of the art and defining future research directions*. 2002, DTIC Document.
- [19] R. Craig Jr, "Substructure methods in vibration," TRANSACTIONS-AMERICAN SOCIETY OF MECHANICAL ENGINEERS JOURNAL OF MECHANICAL DESIGN **117** 207-207 (1995).
- [20] L. Ji, B.R. Mace, and R.J. Pinnington, "A mode-based approach for the mid-frequency vibration analysis of coupled long- and short-wavelength structures," *Journal of Sound and Vibration* **289**(1-2), 148-170 (2006).
- [21] E. Balmès, "Use of generalized interface degrees of freedom in component mode synthesis," *Proceedings of International Modal Analysis Conference*, 1996, pp. 204–210.
- [22] B. Mace and P. Shorter, "A local modal/perturbational method for estimating frequency response statistics of built-up structures with uncertain properties," *Journal of Sound and Vibration* **242**(5), 793-811 (2001).
- [23] M. Ouisse, L. Maxit, C. Cacciolati, and J.L. Guyader, "Patch transfer functions as a tool to couple linear acoustic problems," *Journal of Vibration and Acoustics* **127**(5), 458-466 (2005).
- [24] G. Veronesi, C. Albert, E. Nijman, and J. Rejlek, Patch transfer function approach for analysis of coupled vibro-acoustic problems involving porous materials. 2014,

SAE Technical Paper.

- [25] V. Meyer, L. Maxit, J.L. Guyader, and T. Leissing, "Prediction of the vibroacoustic behavior of a submerged shell with non-axisymmetric internal substructures by a condensed transfer function method," *Journal of Sound and Vibration* **360** 260-276 (2016).
- [26] Z. Hu, L. Maxit, and L. Cheng, "Convergence criteria on the acoustic velocity continuity in a panel-cavity system," *The Journal of the Acoustical Society of America* **141**(3), 2137-2142 (2017).
- [27] R.S. Langley and P. Bremner, "A hybrid method for the vibration analysis of complex structural-acoustic systems," *The Journal of the Acoustical Society of America* **105**(3), (1999).
- [28] L. Tang, L. Cheng, H. Ji, and J. Qiu, "Characterization of acoustic black hole effect using a one-dimensional fully-coupled and wavelet-decomposed semi-analytical model," *Journal of Sound and Vibration* **374** 172-184 (2016).
- [29] L.P. Franzoni and D.S. Labrozzi, "A study of damping effects on spatial distribution and level of reverberant sound in a rectangular acoustic cavity," *The Journal of the Acoustical Society of America* **106**(2), 802-815 (1999).